M. Paula Denofrio, Jose M. Paredes, Juan G. Yañuk, Maria D. Giron, Rafael Salto, Eva M. Talavera, Luis Crovetto and Franco M. Cabrerizo.Photosensitizing properties and subcellular localisation of 3,4-dihydro-β-carbolines harmaline and harmalol. *Photochemical & Photobiological Sciences* (**2023**) 22:487–501 https://doi.org/10.1007/s43630-022-00328-7

Photosensitizing properties and subcellular localization of *3,4*-dihydro-β-carbolines harmaline and harmalol

*M. Paula Denofrio,[a, b,] * Jose M. Paredes,[c] Juan G. Yañuk [a, b], Maria D. Giron,[d] Rafael Salto,[d] Eva M. Talavera,[c] Luis Crovetto,[c,] * and Franco M. Cabrerizo[a, b,] **

[a] *Instituto Tecnológico de Chascomús (CONICET-UNSAM), Av. Intendente Marino Km 8.2, CC 164 (B7130IWA), Chascomús, Argentina. E-mail:* fcabrerizo@intech.gov.ar

[b] Escuela de Bio y Nanotecnologías (UNSAM)*, Argentina*

[c] *Department of Physical Chemistry, Faculty of Pharmacy, Unidad de Excelencia en Química Aplicada a Biomedicina y Medioambiente (UEQ), University of Granada, Cartuja Campus, 18071 Granada, Spain*

[d] *Department of Biochemistry and Molecular Biology II, Faculty of Pharmacy, Unidad de Excelencia en Química Aplicada a Biomedicina y Medioambiente (UEQ), University of Granada, Cartuja Campus, 18071 Granada, Spain*

* To whom correspondence should be addressed (fcabrerizo@intech.gov.ar, pdenofrio@intech.gov.ar and luiscrovetto@ugr.es)

ABSTRACT

Harmaline (**1**) and harmalol (**2**) represent two *3,4*-dihydro-β-carboline (DHβCs) most frequently reported in a vast number of living systems. Fundamental aspects including the photosensitizing properties, cellular uptake, as well as the cyto- and phototoxicity of **1** and **2** were investigated herein. The molecular basis underlying the investigated processes are elucidated. Data reveal that both alkaloids show a distinctive pattern of extracellular DNA photodamage. Compound **1** induces a DNA photodamage profile dominated by oxidised purines and sites of base loss (AP-sites); whereas **2** mostly induces single-strand breaks (SSBs) in addition to a small extent of purine oxidative damage. In both cases, DNA oxidative damage would occur through type I mechanism. In addition, a concerted hydrolytic attack is suggested as an extra mechanism accounting for the SSBs formation photoinduced by **2**. Subcellular internalisation, cyto- and phototoxicity of **1** and **2** and the corresponding full-aromatic derivatives harmine (**3**) and harmol (**4**) also showed quite distinctive patterns in a structure-dependent manner. These results are discussed in the framework of the potential biological, biomedical and/or pharmacological roles reported for these alkaloids.

Keywords: DNA damage, phototoxicity, partially hydrogenated β-carboline, alkaloids, harmol, harmine, cellular uptake, lysosomes, endoplasmic reticulum

This publication is dedicated to Prof. Silvia E. Braslavsky, a pioneer in photobiology and photobiophysics, on the occasion of her 80th birthday.

INTRODUCTION

3,4-dihydro-β-carbolines (DHβCs) comprise a set of natural products present in vast range of living organisms, including mammals. [1-4] Biosynthesis of DHβCs involves the Pictet-Spengler reaction catalysed by strictosidine synthases,[5] and followed by different enzymatic and non-enzymatic reactions to yield the extensive set of DHβCs and full aromatic derivatives (βCs) found in nature. [6] Harmaline (**1**) and harmalol (**2**) (**Scheme 1**) are two of the most representative DHβCs showing a broad spectrum of biological and pharmacological activity:

(i) DHβCs **1** and **2** showed antitumor and antimicrobial activity against a broad spectrum of cell lines and species. [7-12]

(ii) Due to their stimulatory effect on the cellular melanin biosynthesis as well as on the tyrosinase activity, these two DHβCs were suggested to be useful drugs for the treatment of hypopigmentation related skin disorders such as vitiligo. [13] However, the lack of pigmentation might enhance the sunlight exposition of **1** and **2**, triggering photosensitized processes and causing unwanted side effects. Thus, the photosensitizing properties of photoexcited DHβCs need to be investigated.

(iii) Lee *et al.* demonstrated that **1** and **2** have a protective effect on oxidative neuronal damage in mice treated with the neurotoxin MPTP (1-methyl-4-phenyl-1,2,3,6-tetrahydropyridine). In addition, both alkaloids would prevent dopamine-induced mitochondrial damage and PC12 cell death. Both alkaloids would exert their effects at the mitochondrial domain through a scavenging action on reactive oxygen species and inhibition of monoamine oxidase and thiol oxidation. [14] It is noteworthy that the latter *in vitro* study was performed with brain homogenates and/or with isolated mitochondria. In this context, identifying the actual subcellular localization of **1** and **2** becomes relevant to shed light on the mechanism of action suggested.

To gain further insight regarding the molecular bases of the above-mentioned processes, fundamental aspects related to the photosensitizing properties of **1** and **2**, under both extra- and intracellular conditions, are investigated herein. For comparative reasons, data obtained for the corresponding full-aromatic derivatives harmine (**3**) and harmol (**4**) are also reported. [6, 10, 15-23]

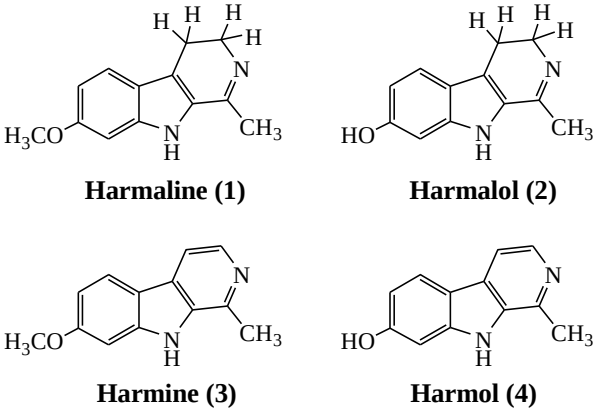

Scheme 1. Chemical structures of βCs studied in this work.

EXPERIMENTAL

General

Reactants: harmine (> 99%), harmaline (> 98%), harmol (> 99%), harmalol (> 98%), phosphate buffered saline medium (PBS, Sigma-Aldrich P5493) and calf thymus DNA (ctDNA, sodium salt type I, highly polymerized, Lot no. 105K7025) from Sigma-Aldrich were used without further purification. The concentration of βCs and ctDNA stock solutions was determined by UV-visible absorption spectroscopy considering molar extinction coefficient values in acidic aqueous solution of 20,656 $M^{-1}cm^{-1}$ (at 372 nm), 15,900 $M^{-1}cm^{-1}$ (at 372 nm), 7,858 $M^{-1}cm^{-1}$ (at 350 nm), 18,965 $M^{-1}cm^{-1}$ (at 320 nm) and 15,800 $Mbp^{-1}cm^{-1}$ (at 260 nm) for **1**, **2**, **3**, **4** and ctDNA, respectively.[16, 23, 24] DNA from bacteriophage PM2 (PM2 DNA, 10^4 bp) was prepared according to the method of Salditt *et al.*[25]

Enzymes: Formamidopyrimidine-DNA glycosylase (Fpg) was obtained from *E. coli* strain JM105 harbouring plasmid pFPG230 [26]. Endonuclease IV (Endo IV) and T4 endonuclease V (T4 endo V) were partially purified from an inducible overproducer (*E. coli* strain A 32480 carrying the plasmid ptac-denV) provided by L. Mullenders, Leiden. Endonuclease III (Endo III) from *E. coli* was kindly provided by S. Boiteux, Fontenay aux Roses, France. All repair endonucleases were tested for their incision at reference modifications according to the procedure described elsewhere [27].

Cell cultures and preparations: Human epithelioid cervix carcinoma (HeLa, ATCC: CCL-2) and HEK293 cells (ATCC: CRL-1573) were provided by the Cell Culture Facility of the University of Granada. Cell cultures were grown at 37°C in a humidified 5% CO_2 incubator in Dulbecco's Modified Eagle's Medium (DMEM) without phenol-red supplemented with 10% (v/v) foetal bovine serum (FBS), 2 mM glutamine, 100 U/mL penicillin, and 0.1 mg/mL streptomycin. Cells were seeded in 6-well plates with a density of 11,250 cells/cm^2 on 25 mm coverslips to reach a 70-80% confluence.

Binding studies

UV-vis spectrophotometric analysis. The interaction of **1** and **2** with calf thymus DNA (ctDNA) was studied by UV-vis absorption spectroscopy according to the methodology described elsewhere. [28] Briefly, spectra were recorded on a Perkin Elmer lambda 25 spectrophotometer. Measurements were made in quartz cells of 1 cm optical-path length, at room temperature. The concentrations of βC phosphate buffer solutions were 25 μM at pH 7.4. ctDNA concentration varied from 0 to 610 μM. Assuming a 1:1 stoichiometry for complexes, the association constants (K_G) was estimated by using the following equation:

$$\frac{1}{\Delta A} = \frac{1}{(\varepsilon_{\beta C\bullet B} - \varepsilon_{\beta C})} \frac{1}{[\beta C]_o} + \frac{1}{K_G\ (\varepsilon_{\beta C\bullet B} - \varepsilon_{\beta C})\ [\beta C]_o} \frac{1}{[B]} \qquad (1)$$

where $\varepsilon_{\beta C\bullet B}$ and $\varepsilon_{\beta C}$ are the molar absorption coefficients of βC•ctDNA complex (βC•B) and βC, respectively, at the titration wavelength. ΔA is the change of absorbance, at ctDNA concentration ([B]), relative to the completely free βC ([βC] = 0 M) at this wavelength. The corresponding K_G values are obtained from the ratio of the slope and intercept of eq. 1.

Fluorescence measurements. Steady-state fluorescence emission was measured using a Fluoromax4 (HORIBA Jobin Yvon). Corrected fluorescence emission spectra were recorded in a 1 cm x 1 cm path lengths quartz cell at room temperature. For determining the quenching of fluorescence of βCs by ctDNA, emission spectra of air-equilibrated βC solutions (25 μM, in phosphate buffer at pH 7.4) were recorded in the absence and in the presence of ctDNA (from 0 to 710 Mbp). To avoid interferences due to changes in the absorbance of the samples because of the βC•ctDNA complex formation, spectra were excited at the corresponding isosbestic points (**Table 1**). The fluorescence intensity (I_F) was obtained by integration of the corrected fluorescence spectra over the entire emission profile.

DNA photoproducts characterization

Irradiation set-up. A mixture of βC buffered aqueous solutions (10 mM KH_2PO_4, 50 mM NaCl, pH 7.4) and PM2 DNA (10 μg/ml) were irradiated for 20 min on ice in a 96 well-plate with a UVA Philips HPW 125W lamp emitting at 365 ± 20 nm, placed at 10 cm, equivalent to 3 J cm^{-2}. Th. Note that at this excitation wavelengths all the investigated βCs show quite high absorption coefficients, ε, [17, 18] whereas DNA absorption is negligible. Treated DNA was precipitated by ethanol/sodium acetate and subsequently dissolved in BE1 buffer (20 mM Tris–HCl, pH 7.5; 0.1 M NaCl and 1 mM EDTA) for damage analysis.

Quantitative analysis of endonuclease-sensitive modifications. The use of DNA (supercoiled extracellular DNA of bacteriophage PM2) relaxation assay, in combination with incision repair endonucleases, to characterise the DNA photosensitized damage has been previously described. [21] Briefly, this assay makes use of the fact that supercoiled PM2 DNA is converted by either a SSB or the incision of a repair

endonuclease into a relaxed (nicked) form, which migrates separately from the supercoiled form in agarose gel electrophoresis. [29] This methods allows the evaluation of several types of putative photosensitizing mechanisms.[22, 29] In this work, four different DNA repair enzymes were used: ***(i)*** formamidopyrimidine-DNA repair glycosylase or Fpg to detect oxidatively damaged purines and AP-sites, ***(ii)*** Endo III to recognize oxidised pyrimidines as well as AP sites, ***(iii)*** T4 endo V to recognize cyclobutane pyrimidine dimers (CPDs) and several specific types of AP-sites, and ***(iv)*** Endo IV to sense all types of AP-sites.

The number of cyclobutene pyrimidine dimers ($CPDs^{calc}$) were calculated as the difference between the number of sites recognized during incubation with both Endo IV and T4 endo V and the number of AP sites recognized by Endo IV alone. Likewise, the number of oxidatively generated damage on pyrimidine nucleobases ($Ox\text{-}Py^{calc}$) were calculated by combining the use of both Endo III and Endo IV enzymes. To further identify the photosensitized DNA damage, two different control experiments were carried out: *light-controls* (PM2 DNA irradiated in the absence of βCs. See data points at the y-intercept in **Figure 1a**) and *dark-controls* (mixtures of PM2 and βCs, at the highest concentrations, kept in the dark).

Fluorescence Imaging Microscopy

FLIM experiments were carried out on a MicroTime 200 instrument (PicoQuant), using an LDH-375 (PicoQuant) pulsed laser as an excitation source with a repetition rate of 20 MHz. The laser was directed into the sample using a dichroic mirror (F33-375RDC, AHF/Chroma) and an oil immersion objective (1.4 NA, 100×) of an inverted microscope (IX-71, Olympus). The emitted fluorescence was filtered by a cut-off filter (F76-405LP, AHF/Chroma) and focused onto a 75 μm pinhole. The detection filter was a FB450-40 bandpass filter (Thorlabs), and the fluorescence was detected using a single-photon avalanche diode (SPCM-AQR 14, PerkinElmer). Photon counting, imaging reconstruction and data acquisition were performed with a TimeHarp 200 TCSPC module (PicoQuant). Raster scanned images were recorded with a 512 × 512 pixels resolution. The fluorescence images were analysed using the image processing package Fiji. [30] For live-cell experiment samples were prepared as follow: HeLa and HEK293 cells grown on coverslips (in DMEM) were washed (2 times) with phosphate buffered saline medium (PBS), then incubated with the corresponding βC in PBS solution (extracellular concentration = 10 - 12 μM) at 37°C. *Colocalization studies* were performed in an Abberior scanning microscope (Abberior Instruments GmbH, Germany) equipped with a 375 nm, 560 nm, and 640 nm source lasers. Excitation were sequentially switched between 375 nm and 560 nm (or 640 nm) to excite the βC and the biomarkers, respectively. Emission signals were recorded in two different emission ranges: 495 – 520 nm, and 580 - 630 nm (or 640 - 750 nm), to collect the βC (cyan channel) and the biomarkers (red channel) fluorescent emission,

respectively. The objective used was an UPlanSApo 100×/1.40 oil immersion. In all the measurements, the pinhole size was set to 1 AU (Airy unit). For samples prepared, HeLa cells in DMEM free of FBS were first incubated with Mitotracker®, Lysotracker® and ER-Tracker (16 nM) in three different sets of experiments. After 20 min incubation, βC (10 μM) was added and co-incubated during 2 h. Cells were then prepared for confocal microscope analysis.

Cytotoxicity effect of 1 to 4 on A549 cells

The viability of host cells after treatment with the investigated βCs was evaluated by using the colorimetric MTT (3-[4,5-dimethylthiazol-2-yl]-2,5-diphenyltetrazolium bromide) assay as it was described elsewhere. [15] Briefly, A549 cells were trypsinized, counted and seeded into 96-well culture plates at a density of 15,000 - 20,000 cells/well and grown in supplemented DMEM without phenol-red to confluence for 24 h. Cells were then exposed to several dilutions of the assayed compounds. Control cells (*negative control*) were treated with the same volume of dimethyl sulfoxide (DMSO) as vehicle alone (final DMSO concentration was 0.5%). To avoid effects of evaporation, outer wells were not used. After 24 h or 48 h of incubation with the βC, medium was removed, cells were washed with phosphate buffer saline (PBS) and treated with 0.5 mg/mL (100 μL/well) of the tetrazolium dye MTT (*3*-(*4,5*-dimethylthiazol-*2*-yl)-*2,5*-diphenyltetrazolium bromide, Sigma-Aldrich) in PBS, during 3 h, at 37 °C and 5% CO_2. Supernatants were removed, and formazan crystals were solubilized in DMSO (100 μL/well). Absorbance at 540 nm (reference wavelength: 700 nm) was read in a plate reader (Synergy H1 Hybrid Reader, Biotek). Average absorbance from background wells (without cells, treated as the samples), was subtracted out, to obtain corrected values ($A_{540\ corr}$). The percentage of cell viability was calculated as:

$$\text{Cell viability (\%)} = (A_{540\ corr\ (treated\ cells)}) / (A_{540\ corr\ (untreated\ cells)}) \times 100 \quad (2)$$

CC_{50} values were obtained by non-linear regression analysis of Cell Viability (%) vs. Log [βC] with a variable Hill's slope (normalized response), using GraphPad Prism 5.03 software. Each concentration was assayed in triplicates, in five independent sets of experiments.

Phototoxicity of 1 and 2 on A549 cells.

A549 cells were counted and seeded into 96-well culture plates at a density of 20,000 cells/well and grown to confluence for 24 h following the procedure described above. Cells were incubated with DHβC in DMEM (without phenol-red) for 1.5 h. After incubation, cells were irradiated (Rayonet lamp @420 ± 20 nm, 2 J cm^{-2}) for 10 min and then were incubated during 24 h prior the determination of cell viability by MTT assay as it was described above.

RESULTS AND DISCUSSIONS

DNA damage induced by photoexcited DHβCs under cell-free conditions

The photosensitizing properties of **1** and **2** (**Scheme 1**) were explored herein using supercoiled extracellular DNA of bacteriophage PM2, in combination with a set of four incision repair endonucleases. The dose-dependence of the DNA damage was investigated first (**Figure 1a**) by exposing PM2 to a fixed dose of UVA (365 ± 20 nm, 3 J/cm^2), in the presence of various concentrations of **1** and **2**. The number of single-strand breaks (SSBs) and modifications sensitive to Fpg were subsequently quantified. Interestingly, despite both compounds showed a linear dose-dependence trend, a distinctive behaviour was observed for each case. Compounds **1** showed the typical dose-dependence already reported for other related full-aromatic βCs, including **3**. [19-22, 28, 31-35] Briefly, Fpg-sensitive sites (*i. e.*, oxidatively modified purines including *8*-oxo-*7,8*-dihydroguanine and formamidopyrimidines, as well as sites of base loss or AP sites) were found to be produced with higher efficiency than SSBs. On the contrary, **2** showed the opposite trend. In all the cases, DNA damage observed is mediated by the photoexcited βCs, since no damage was observed in both *light*- and *dark controls*.

Minor chemical modifications of the molecular structure of the βC-ring can dramatically modify its photodamage pattern and, as such, the DNA damage profile.[16, 19, 22] Therefore, the number of four types of repair enzymes-sensitive modifications (*i.e.*, DNA damage profile) photoinduced by **1** and **2** were additionally determined (**Figure 1b**). Data evince a strong qualitative and quantitative structure-activity relationships:

(*i*) Both **1** and **2** induce specific DNA base damage. In the case of **1**, the damage profile observed is characterised by a relatively high number of oxidatively damaged purines and AP-sites (*i. e.*, Fpg-sensitive base modifications). This is consistent with the fact that DHβCs bind preferentially with dG•dC rich DNA regions. [36, 37] Sites of base loss or AP-sites, which are specifically recognized by endonuclease IV, and SSB are generated in lower amounts. On the contrary, SSBs represent the main types of DNA damage when the genetic material is irradiated in the presence of **2**.

(*ii*) It is generally accepted that Fpg-sensitive sites are produced either by type I (via electron transfer) or type II (via reactive oxygen species such as singlet oxygen, $^1O_2$) photosensitization mechanisms.[29] Taking into account the extremely low or null efficiency of singlet oxygen production ($\Phi_\Delta \sim 0.02$) showed by both **1** and **2**, [23] type I would be the operative mechanism in the Fpg-sensitive sites photosensitized formation. The extended oxidative damage depicted by non-negligible amounts of Endo IV sensitive sites photoinduced by both DHβCs further support this hypothesis.

(*iii*) When considering the oxidation potential of **1** (0.532 V vs. Ag-AgCl) and **2** (0.328 V vs. Ag-AgCl) (**Figure SI.1**), as well as the vibrational zero electronic energies (*i. e.*, $\Delta E_{0,0}$ of 2.91 eV for both compounds), a slightly larger extent of DNA photooxidative damage is expected for **1** (**Figure SI.2**). This is evident when comparing the slopes of Fpg-sensitive sites depicted in **Figure 1a**.

(*iv*) SSBs can be formed from a cumulative damage on the DNA moiety. However, this does not seem to be the case for compound **2**, where a relatively large amount of SSBs is observed since the very early stage of the reaction (**Figure 1b**). In a recent work, a concerted photoinduced hydrolytic attack of the DNA was suggested as the operative mechanism responsible for SSB formation photoinduced by a related βC derivative (6-chloroharmine).[22] This could also be the case for **2**. Note that the acidity of both -N(9)H and -OH group placed at C(7) of **2** are enhanced when subject to photoexcitation.[23] This is more evident when analysing the electronic density over the molecule depicted in the molecular orbital diagrams reported by Villarruel *et. al* [23] and from the emission spectra depicted in **Figure SI.2** and **Table SI.1**. Therefore, upon photoexcitation, **2** may induce a drastic change in the local pH, yielding in a hydrolytic attack that might give rise to SSB and/or AP-site formation. This hypothesis is further discussed below (**Figure 2**).

(*v*) Data obtained by using a combination of Endo III, T4 Endo V and Endo IV show that other types of DNA damage such as CPDs and oxidised pyrimidines (Ox-Py^{calc}) are absent or generated in rather low relative yields, respectively. This contrasts with the broader DNA damage spectra previously determined for certain full-aromatic βCs such as **3**.[19, 29] Photosensitized formation of CPDs mainly occurs through triplet–triplet energy transfer (TTET) from the triplet electronic excited state of the photosensitizer to the triplet electronic state of the pyrimidine (mostly, thymine). Considering the thermodynamic restrictions for this process to occurs (*i.e.*, photosensitizers must have energy triplet values (E_T) larger than 267 kJ mol^{-1}), [38] the lack of CPDs formation suggest that both investigated DHβCs (**1** and **2**) do not have the required energy for triplet-triplet sensitization. Although the E_T value of **1** and **2** are unknown, the large changes in the relative energy of their electronic states (*i. e.*, bathochromic shift ~ 30 nm)[23] with respect to the full-aromatic derivatives **3** and **4**, respectively, support this conclusion.

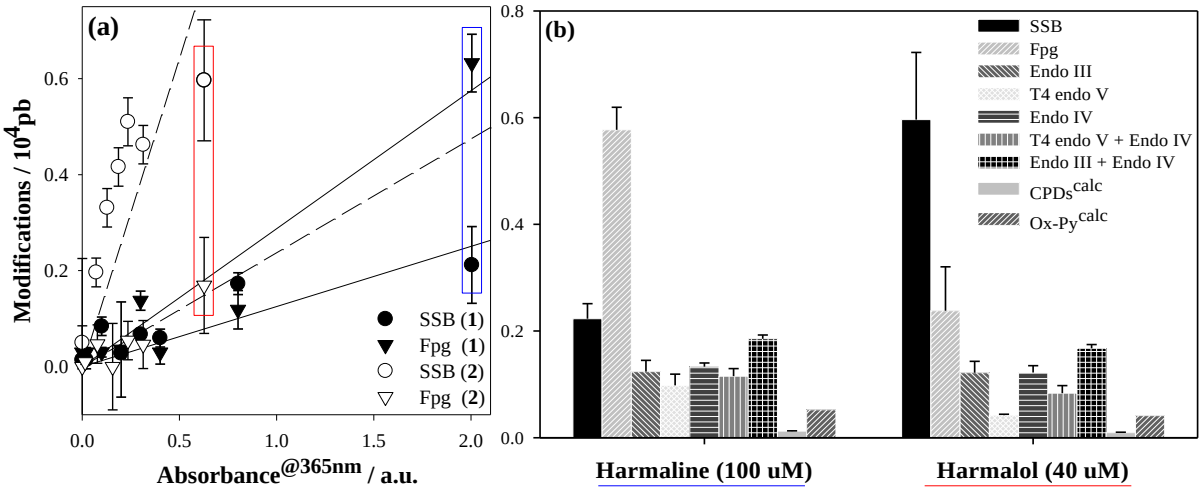

Figure 1. (a) DNA single strand breaks or SSBs (circles) and modifications sensitive to Fpg protein (down triangles) induced in PM2 DNA by exposure to UVA (365 ± 20 nm) in the presence of different concentrations of **1** (black) and **2** (white) in phosphate buffer solutions (pH 7.4). For comparative purposes, concentrations are plotted in *x*-axis as absorbance at the excitation wavelength ($Abs^{@365nm}$). Data are means of 3 independent experiments (± S.D.). **(b)** DNA damage profiles showing the numbers of SSBs, and several types of endonuclease sensitive modifications induced in PM2 DNA by photoexcited DHβCs **1** (100 μM, $\varepsilon_{@365nm}$ = 20,040 $M^{-1}cm^{-1}$) and **2** (40 μM, $\varepsilon_{@365nm}$ = 15,680 $M^{-1}cm^{-1}$). Data are the means of 3 independent experiments (± S.D.).

Interaction between 2 and 4 with calf thymus DNA

The interaction between **1** and **2** with genetic material, including calf thymus DNA (ctDNA), has been previously described. [16, 36, 37, 39-43] Due to the strong solvent dependence of the photophysical and photochemical properties of βCs, a comparative UV-vis absorption and fluorescence spectroscopic analysis of the interaction between **1** and **2** with ctDNA in phosphate buffered solutions at pH 7.4 (*i. e.*, under the same experimental conditions used in the PM2 experiments) was performed herein. UV-vis spectra of **1** and **2** were recorded in the presence of increasing amounts of ctDNA (**Figure 2**). The spectroscopic pattern observed was the same to that previously reported by Duportail *et al.* [39] and Sarkar *et al.* [43] for **1** and **2**, respectively. Briefly, in the presence of ctDNA, the absorption spectra of both compounds show a large hypochromism and bathochromic shift, accompanied by the appearance of isosbestic points (see λ_{iso} in **Table 1**). The corresponding association constants (K_G) between βCs and ctDNA were obtained from eq. 1 (**Table 1**). Representative plots depicted as insets in **Figure 2** show a linear dependence with the DNA concentration. The comparison of K_G values confirms results previously reported suggesting that, in the electronic ground state, the interaction of **1** with ctDNA is slightly stronger than that observed for **2** ($K_G^{\mathbf{1}} > K_G^{\mathbf{2}}$). [39] When comparing the binding constants reported herein, it appears very clearly that DHβCs show lower affinity to ctDNA than the corresponding full-aromatic derivatives **3** and **4**. [19, 37] Thus, the hydrogenation of a double bond at C(3)-C(4) of the pyridine ring in the DHβCs greatly reduces the extent of interactions.

Steady-state fluorescence spectroscopy was used to further analyse the interaction between βCs (in both the electronic ground (S_0) and excited states (S_1)) and ctDNA. Emission spectra of **1** and **2** were recorded in the presence of increasing amounts of ctDNA (**Figures 2c** and **d**). The increase in the ctDNA concentration causes a decrease in the fluorescence intensity of both alkaloids. Interestingly, in the case of **2**, the shape of the emission spectra changes with the increase of the ctDNA concentration. This is more evident when comparing the normalised emission spectra shown as inset in **Figure 2d**. Briefly, changes in the relative intensity of the bands ascribed to the cationic (**C*** ~ 480 nm) and zwitterionic (**Z(II)*** ~ 540 nm) species (**Figure SI.3**)[23] are evident. Thus, the presence of proton acceptors/donor groups (*e. g.*, DNA nucleobases) affect the equilibria among the different acid-base and/or prototropic species of **2** changing their steady-state relative concentrations. Such a proton exchange might induce shifts in the local pH that can lead to the hydrolysis of DNA phosphodiester-bounds with the concomitant SSBs formation. The latter hypothesis deserves to be further investigated with additional spectroscopic and analytical techniques.

In both cases a linear trend was observed in the Stern-Volmer plots (not shown) and the corresponding slopes values ($K_{SS} = \tau_F \, k_q^F$) obtained are listed in **Table 1**. Bearing in mind the βCs fluorescence lifetime (~ 5 – 6 ns) [23] values of ~ 10^{11} M^{-1} s^{-1} can be calculated for the bimolecular quenching constant (k_q^F). This fact suggests a large contribution of a static quenching between βCs and ctDNA. When comparing the magnitude of K_{SS} values it is evident that **1** shows a stronger interaction than **2** ($K_{SS}^{\mathbf{1}} > K_{SS}^{\mathbf{2}}$). This trend agrees with that one observed from the UV-visible spectroscopic titration. It is worth mentioning that despite both techniques show values that are in the same order of magnitude for each compound, values are slightly different. This could be accounted for the fact that in the fluorescence experiments other processes can be detected in addition to the formation of a ground state complex. Another key aspect that might also explain the difference is the fact that both compounds are producing fluorescent βC•ctDNA complexes. [39] This is clear when analysing the evolution of the absorbance and emission intensity as a function of the ctDNA concentration that a plateau is reached at the highest ctDNA concentration (**Figure SI.4**).

Regarding the mode of action, circular dichroism studies suggest that intercalation of **1** into the stacked base pairs of double-stranded DNA is unlikely. The lack of full planarity in the DHβC moiety would be the reason for this behaviour. [39] On the contrary, the molecule would probably adopt a tilted position in one of the DNA grooves. [40] Another key factor that might also be responsible of a non-intercalative mode of action is the fact that, under these experimental conditions (pH 7.4), the cationic (protonated) species of **1** and **2** are present in the solution. Thus, as it was previously reported, cationic βCs are typically bound parallelly to the DNA base pairs, by partial insertion through the double helix

groove, [41] placing the N(9) atom in a polar-protic environment towards the negatively charged DNA backbone. [16]

Table 1. Benesi-Hildebrand binding constants (K_G) and Stern-Volmer constants (K_{SS}) for static quenching of the fluorescence of compounds **1** and **2** and ctDNA.

		1	**2**
UV-vis	[a] K_G / M^{-1}	2.9 (± 0.6) x 10^3	0.7 (± 0.2) x 10^3
	[b] λ_{iso} / nm	314 and 395	310, 402 and 444
Emission	[c] K_{SS} / M^{-1}	1.9 (± 0.3) x 10^3	0.9 (± 0.2) x 10^3

[a] Data obtained from UV-vis spectroscopy analysis (Benesi-Hildebrand correlation).
[b] λ_{iso} is the wavelength of the isosbestic points in UV-vis spectra (nm).
[c] and [d] Stern-Volmer constants obtained from steady-state measurements. Samples were excited at the low energy isosbestic point ($\lambda_{exc} = \lambda_{iso}$).

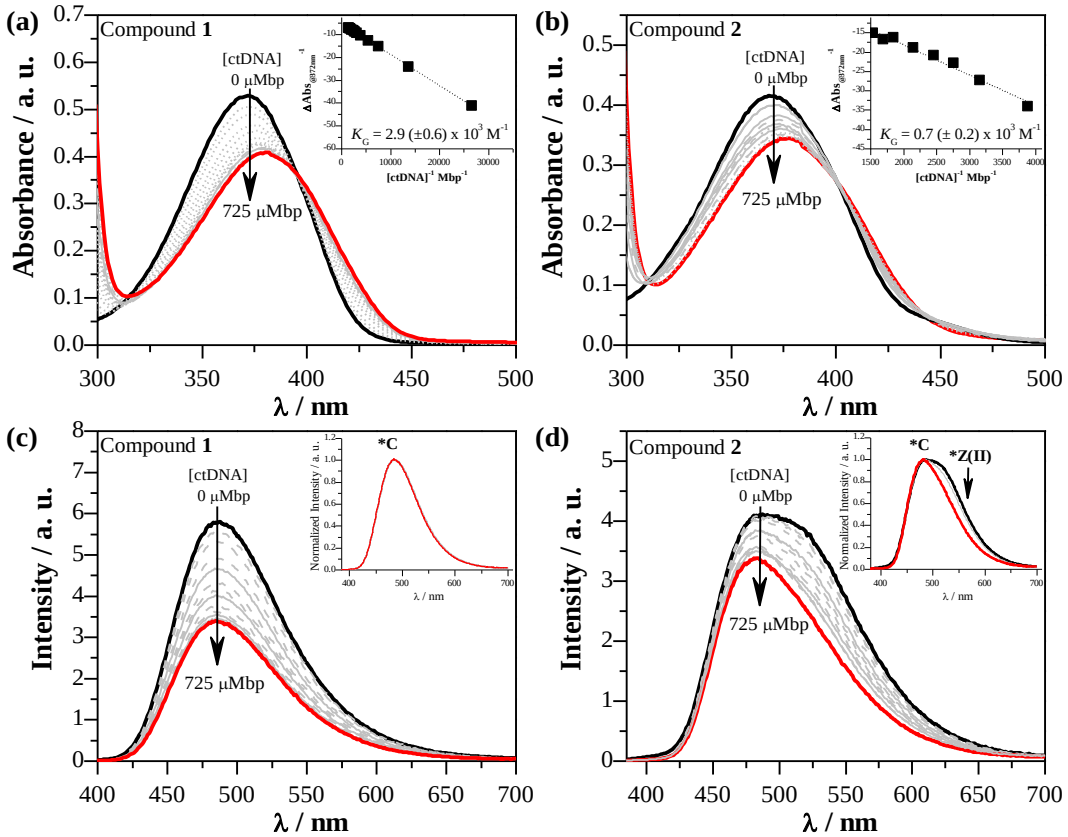

Figure 2. (a) and **(b)** UV-vis absorption spectra of **1** and **2** (25 μM, phosphate buffer solution at pH 7.4), respectively, in the presence of increasing amounts of ctDNA (see arrows). Insets depict representative examples of Benesi-Hildebrand plots (eq. 1). **(c)** and **(d)** Fluorescence emission spectra of **1** and **2** buffered solution (25 μM), respectively, recorded in the presence of increasing amounts of ctDNA at pH 7.4. Arrows indicate the variation in the [ctDNA] in Mbp. Samples were excited at the low energy isosbestic point (λ_{iso}) (**Table 1**). *Insets*: normalised emission spectra.

Cellular uptake of βCs

The cellular internalisation of a particular group of full-aromatic βCs was recently investigated by FLIM microscopy, [16] showing that mild changes in the βC ring (*i. e.*, *N*-methylation) modulate both the dynamics of the drug uptake (and release) by HeLa and HEK293 cells as well as the intracellular

localization. Having this in mind, the cellular uptake of the two DHβCs **1** and **2** as well as their respective full-aromatic derivatives **3** and **4** was investigated herein (**Figures 3**, **SI.5** and **SI.6**).

When co-incubated with βCs in PBS, cells were able to take up all four investigated compounds within 25 - 40 min depending on the chemical structure (**Figure SI.5**). In the case of both *3,4*-dihydro-derivatives (**1** and **2**), the maximum emission intensity (plateau) is reached 10 - 15 min later than their respective full-aromatic derivatives (**3** and **4**). This fact would be compatible with a passive uptake mechanisms where a reduced cellular membrane permeability is expected for polar cationic species.[16] Note that **1** and **2** show pK_a values up to 2-times larger than **3** and **4**, respectively.[18, 23] Thus, under physiological pH conditions protonated (cationic) species of **1** and **2** are present in more than 99.9%, whereas ~50% - 60% of **3** and **4** are present in the neutral form. Additional experiments are needed to further address the actual uptake mechanism.

Interestingly, two distinctive image patterns were observed (left column in **Figures 3** and **SI.6**). The four compounds investigated stain the same intracellular structures, including additional stain of intranuclear structures (see below). This is more evident for both compounds bearing a hydroxyl group at C(7) (*i. e.*, **2** and **4**). The second column in **Figures 3** and **SI.6** show the lifetime images from the entire cells. The corresponding histograms showing the changes in intensity and lifetime along the arrow traced in the first and second columns are depicted in the third column of **Figures 3** and **SI.6**. At a first glance, the four compounds show quite a similar histogram pattern. *I. e.*, the regions showing the highest fluorescence intensity show the lowest fluorescence lifetimes (τ_F). This agrees with the fact that fluorescence properties of βCs **1** - **4** strongly depend on the environment. [6, 18, 23, 44] Briefly, in polar-protic solvents, photoexcited cationic species (**C***) of βCs is the dominant emitting species, showing τ_F values of ~5 ns (*e. g.*, in water τ_F = 5.9 ns and 4.7 ns for compounds **1** and **2**, respectively). On the contrary, in non-protic solvents photoexcited neutral species (**N***) of βCs is the main emitting species showing slightly larger τ_F values (*e. g.*, in ACN or DMSO τ_F of ~ 7 ns [44] and 6.0 ns for compounds **1** and **2**, respectively). In this context, data depicted in the histograms (**Figure 3**) would be compatible with a model where βCs alkaloids would be sensing a polar-protic environment (aqueous media in the interior of the organelles) and, to a lower extent, a non-protic environment (cellular membranes). Moreover, the fact that the fluorescence quantum yield (Φ_F) of DHβC in aqueous environment is lower than in organic solvents [44] support the hypothesis that the highest fluorescent intensity regions depicted in the histograms represent the subcellular domain where the alkaloids accumulate n greater proportion (see below).

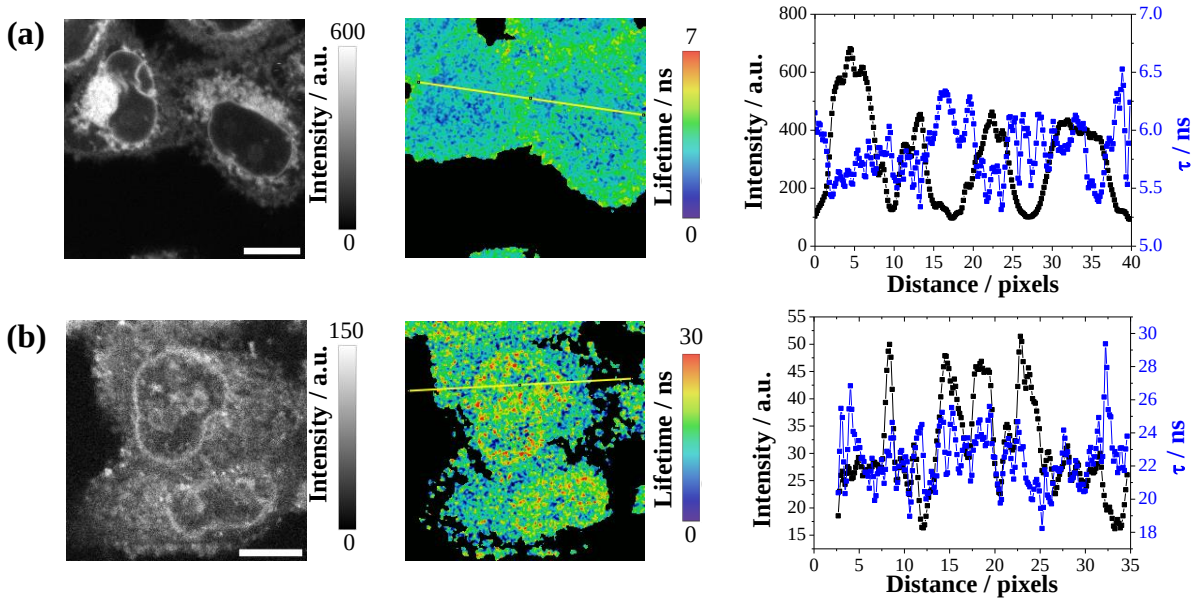

Figure 3. Fluorescence images of HeLa cells incubated with **(a) 1** and **(b) 2**. *Column 1:* fluorescence intensity images of βCs (λ_{exc} = laser at 375 nm, λ_{em} 495 - 520 nm). *Column 2*: fluorescence lifetime images of dye in the whole cell. *Column 3*: plot of intensities and average lifetimes along the selected arrows (histograms). Scale bars represent 10 μm.

Intracellular localization of **1** to **4** was further characterised by using three different red fluorescent biomarkers Lysotracker®, Mitotracker® and ER-Tracker, that selectively stain mitochondria, lysosome, and endoplasmic reticulum, respectively (**Figures 4, SI.7** and **SI.8**). The investigated compounds showed two distinctive localization patterns depending on the chemical nature of the substituent placed at C(7) (*i. e.*, -OCH_3 or -OH). This is better represented by the white pixels in the merged images, and it is also accounted for by the Pearson's coefficients depicted in **Figure 4c**. Briefly, **1** and **3** showed quite a large localization in the lysosomes (R ~ 0.5 - 0.7) and endoplasmic reticulum (R ~ 0.4) and, to some extent, a minor colocalization in the mitochondria (R ~ 0.15). On the contrary, **2** and **4** showed quite a homogenous distribution among the three investigated subcellular organelles (*i. e.*, R ~ 0.3, ~ 0.2 and ~ 0.2 for lysosomes, endoplasmic reticulum, and mitochondria, respectively). Interestingly, R values for Lysotracker® and ER-Tracker observed for **2** and **4** were slightly lower than the corresponding values observed for **1** and **3**. This fact can be rationalized in terms of the qualitative information depicted in **Figure 3** showing that, although the four investigated βCs are able to stain other subcellular domains (such as intranuclear structures), **2** and **4** showed the highest.

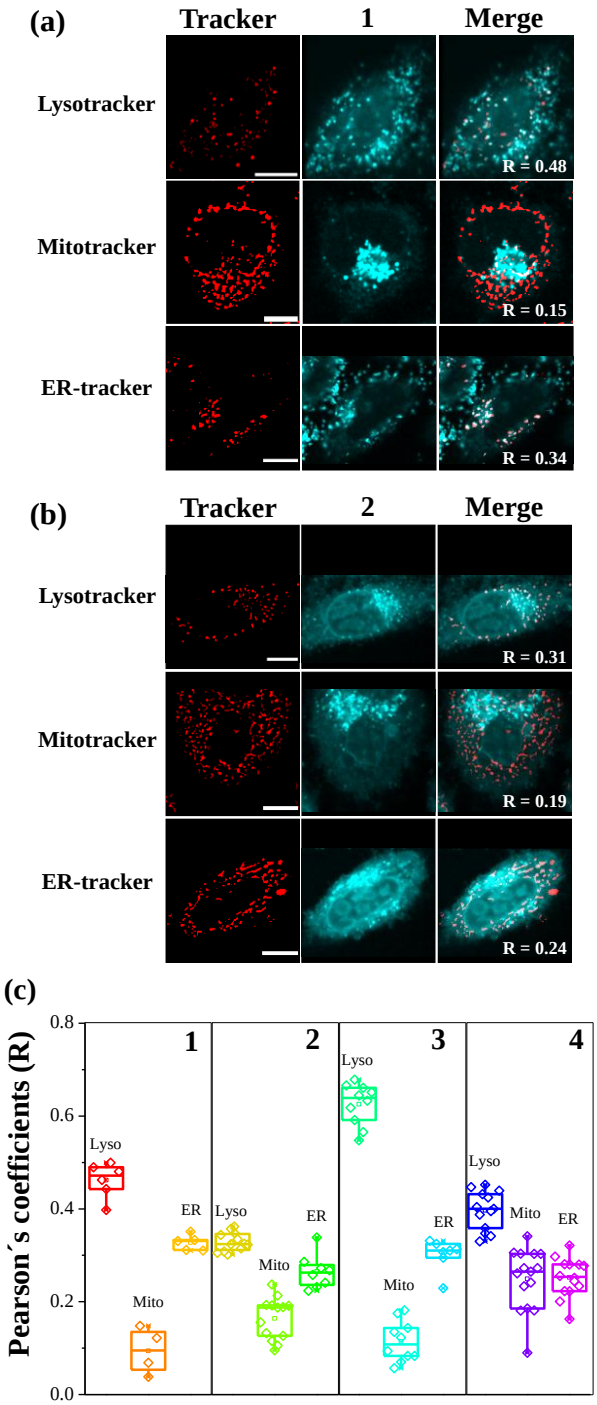

Figure 4. Representative fluorescence images of HeLa cells co-incubated with: **(a) 1** and **(b) 2** with three different biomarkers (Lysotracker®, Mitotracker® and ER-Tracker). White pixels in the merge from the biomarker (*first column* in red) and compound (*second column* in cyan) images depict the colocalization extent (*third column*). **(c)** Pearson´s coefficients calculated for the four alkaloids with the three biomarkers investigated. Scale bars represent 10 µm.

Cytotoxicity of 1 - 4 on eukaryotic cells

The toxicity of these four alkaloids have been largely studied. [15, 36, 45-48] However, these studies were performed under different experimental conditions (incubation times, % of foetal bovine

serum (FBS) and/or % of the vehicle DMSO, etc.), making a direct comparison difficult. All these facts might account for the large variability on the CC_{50} values reported. In this work, the effect of **1** to **4** on the A549 cells' viability was evaluated. Data obtained from dose–response curves (**Figures 5a** and **b**) revealed a strong qualitative and quantitative structure-activity relationship (**Table 2**):

(*i*) Both DHβCs (**1** and **2**) showed lower toxicity on eukaryotic cell culture than their corresponding full-aromatic derivatives **3** and **4** (entry 1). Interestingly, a similar trend has been described for **1** and **3** (entries 5-10) [10, 45] and for **2** and **4** (entries 11-13) [47] on different cell lines including A549.

(*ii*) Among the DHβCs, the presence of the methoxy group placed at C(7) in the βC ring of **1** might enhance the cytotoxicity of the alkaloid (entries 1 and 3). This could be related to the fact that **1** showed a stronger interaction with biomolecules than **2** and/or to the fact that both alkaloids show mild differences in the subcellular internalisation patterns.

(*iii*) The increase in the incubation time (from 24 h to 48 h) of A549 cells treated with **1** and **2** enhances the cytotoxicity of both alkaloids (entries 1 and 4). This is in agreement with results reported by Roy *et al.* (entries 14-15) [46] , Sarkar *et al.* (entries 16-19), [36] and Cao *et al.* (entries 20-25) [48]. Briefly, the larger the incubation time, the lower the CC_{50} values observed.

(*iv*) The total amount of foetal bovine serum (%FBS) used as a supplement in the culture media strongly affects the apparent cytotoxicity of the alkaloids investigated. The higher the %FBS, the lower the cytotoxicity (*i. e.*, the higher the CC50 values observed) (entries 1-3). A similar trend was reported by Ghosh *et al.* [49] The latter fact suggests that βCs might strongly interact with the proteins present in FBS and therefore a lower βC' effective concentration is observed.

(*v*) With the exception of HepG2 (entries 19 and 22) and HBL-100 (entry 7), cytotoxicity of βCs against different cell lines, including A549 and HeLa, is quite similar. This is reflected in the similarity of the CC_{50} values reported for each experimental condition.

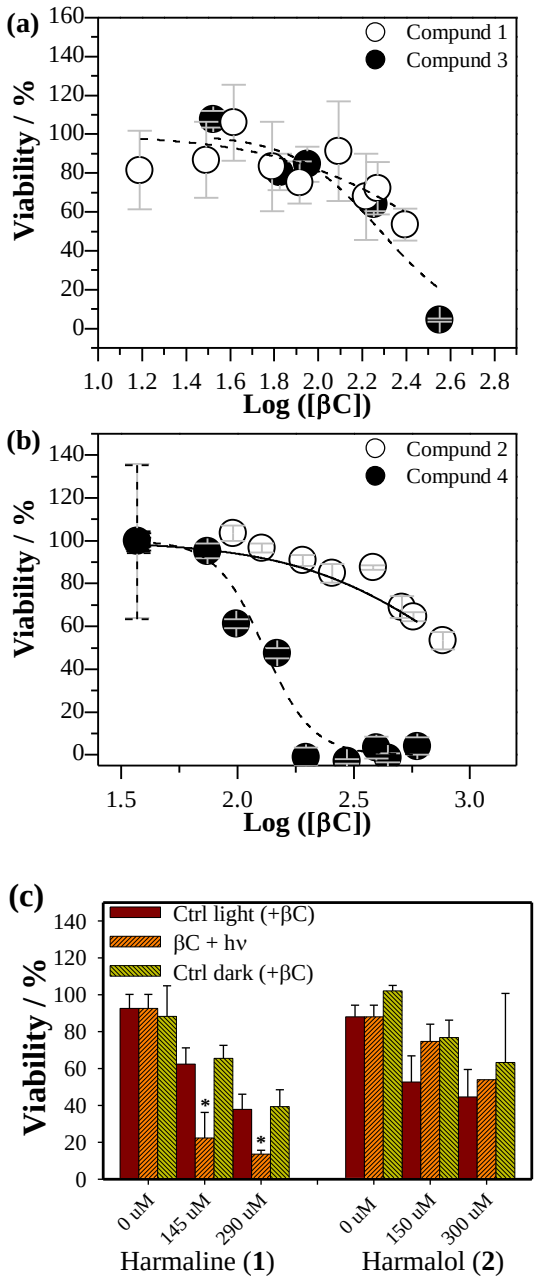

Figure 5. (a) and **(b)** Effect of **1** to **4** treatment in human lung A549 cells. Cells were treated with various concentrations of βCs for 24 h. After culture, cell viability was measured by the MTT (tetrazolium dye) assay. Data are means of 5 independent experiments (±S.D.). **(c)** Phototoxic effect of **1** and **2** against A549 cell culture. Cells were incubated first with different non-cytotoxic βC' concentrations during 3 h. Cells were irradiated (@420 ± 20 nm) for 10 min and then incubated during 24 h. Note that Control-light experiments represent cells irradiated in the absence of βC and then incubated during 24 h in the presence of the alkaloid. Pylons labelled with an asterisk indicate that there are significant differences between this number and the corresponding numbers obtained from the Control-light populations of each assay (one-way ANOVA; $p < 0.05$).

Table 2. Summary of cytotoxicity effect of **1** to **4** obtained under the experimental conditions investigated herein. Cytotoxicity as CC_{50} is the concentration of compound which reduces by 50% the optical density of treated cells with respect to untreated cells using MTT assay (exceptions are duly indicated as footnotes at the bottom of the table). For further comparison data reported in the literature are also listed in the table.

Entry	Cell line	Experimental conditions				CC_{50} (1) / μM	CC_{50} (2) / μM	CC_{50} (3) / μM	CC_{50} (4) / μM	Ref.
		Cells / 10^3 well	Inc. time / h	% FBS	% DMSO					
1	A549	20 (96-well plates)	24	10	0.5	330 ± 70	> 600	230 ± 50	120 ± 20	This work
2		10-15 (96-well plates)	24	5	0.5	--	180 ± 60	180 ± 10	160 ± 30	
3			24	2	0.5	97 ± 7	121 ± 10	--	82 ± 8	
4		20 (96-well plates)	48	10	0.5	215 ± 40	250 ± 20	--	--	
5	[a] Vero	20 (96-well plates)	48	5	1	187 ± 3	--	73.0 ± 0.3	--	[10]
6	A549	20 (96-well plates)	24	10	nr	137 ± 1	--	107 ± 2	--	[45]
7	HBL-100		24	10	nr	38 ± 1	--	32.6 ± 0.7	--	
8	HT-29		24	10	nr	218 ± 3	--	45.6 ± 0.9	--	
9	HeLa		24	10	nr	244 ± 1	--	61.8 ± 0.7	--	
10	HCT-116		24	10	nr	130.0 ± 0.3	--	34.0 ± 0.2	--	
11	[b] A549	60 (48-well plates)	24	nr	0.1	--	Not cytotoxic within the concentration range tested (0 to 100 μM).	--	[d] 100 (85.6%)	[47]
12	[b] H226		24	nr	0.1	--		--	[d] 100 (84.7%)	
13	[b] H596		24	nr	0.1	--		--	[c] ~25 – 30	
14	A549	8-10 (96-well plates)	48	10	nr	68 ± 3	--	--	--	[46]
15	H1299		48	10	nr	48 ± 2	--	--	--	
16	A549	20 (96-well plates)	72	10	0	--	[c] 45.2 (54.0)	--	--	[36]
17	HeLa		72	10	0	--	[c] 42.5 (50.8)	--	--	
18	MDA-MB-231		72	10	0	--	[c] 23.7 (28.3)	--	--	
19	HepG2		72	10	0	--	[c] 14.2 (17.0)	--	--	
20	HeLa	20 (96-well plates)	72	10	2	--	--	60	--	[48]
21	PLA-801		72	10	2	--	--	45	--	
22	HepG2		72	10	2	--	--	46	--	
23	Bel-7402		72	10	2	--	--	54	--	
24	BGC-823		72	10	2	--	--	68	--	
25	Lovo		72	10	2	--	--	66	--	

[a] Determined by MTS (*3*-(*4*,*5*-dimethylthiazol-*2*-yl)-*5*-(*3*-carboxymethoxyphenyl)-*2*-(*4*-sulfophenyl)-*2*H-tetrazolium) assay. [15]
[b] Determined by WST-8 (*2*-(*2*-methoxy-*4*-nitrophenyl)-*3*-(*4*-nitrophenyl)-*5*-(*2*,*4*-disulfophenyl)-*2*H-tetrazolium) assay. [47]
[c] A molar extinction coefficient value of 19,000 M^{-1} cm^{-1} was used to determine the concentration of **1** stock solution. The later value is larger than the one used in the present work (15,904 M^{-1} cm^{-1}). For better comparison, CC50 values reported by Sarkar *et al.* were corrected (by a factor of ~1.2) and depicted between parentheses.
[d] Authors reported the % of cell viability (listed between parenthesis) after treatment with one concentration of **4** only (100 μM).
[e] CC_{50} value estimated from the data reported therein: 25 μM (58.4%), 50 μM (21.2%), 75 μM (13.8%) and 100 μM (1.9%).
nr = information not reported by the authors.

Phototoxicity of 1 - 4 on eukaryotic cells.

Under *in vitro* conditions, **1** and **2** showed quite an important photosensitizing activity (**Figure 1**) as well as intracellular localisation on eukaryotic cells (**Figure 3**) in a dose- and structure-dependent manner. To further evaluate the photodynamic activity on cell culture, A549 cells treated pre-incubated with the DHβCs were irradiated (420 ± 20 nm) during 10 min. Under the experimental conditions explored herein only compound **1** showed a photodynamic effect (**Figure 5c**). This fact can be explained, on one hand, in the framework of the differential mechanisms of photodamage described above for these two DHβCs. A larger oxidative damage is photoinduced by compound **1** comparing with **2** that, upon

photoexcitation, shows an additional and dominant non-oxidative deactivation pathway (*i. e.*, proton exchanges). Considering genetic material as a potential intracellular target, the purine bases oxidation induced by **1** can led to mutations and hence to cell death, whereas SSBs induced by photoexcited **2** represents a type of damage that can be promptly and efficiently reverted by living cells. In addition, photoexcited **1** and **2** can also induce distinctive lysosomes, ER membranes and/or mitochondrial photodamage profiles and/or organelle dysfunction that might trigger differential photodynamic responses. [50] In this context, images of cells acquired 3 h after irradiation in the presence of **1** show a cytoplasmic vacuolization associated with a paraptotic-like response (**Figure SI.9**). [51] Despite this, further studies are needed to clearly assess the mechanism of photodynamic action of these alkaloids.

The potential use of **1** and **2** to treat hypopigmentation disorders (*e. g.*, vitiligo) was suggested by Park *et al.* [13] The results obtained herein, showing a very low cytotoxicity (CC_{50} > 600 μM, **Figure 5b**) and low or null intracellular photodynamic activity (**Figure 5c**), indicate that **2** would be the best candidate for this particular pharmacological application in order to avoid potential photoinduced side effects.

CONCLUSIONS

This work reports a comparative study of the photosensitizing properties of two *3,4*-dihydro-β-carboline alkaloids (DHβCs), harmaline (**1**) and harmalol (**2**), under extracellular and intracellular domain. In addition, the cyto- and phototoxic effects of these alkaloids as well as their subcellular uptake and localization was also investigated. For comparative reasons results obtained for the two full-aromatic related βC harmine (**3**) and harmol (**4**) were included. Data reported herein show that a subtle structural change (*i. e.*, -OCH_3 or -OH substituent at C(7) in the βC ring gives rise to quite distinctive action patterns:

(i) Regarding the extracellular DNA photodamage, **1** mainly induces oxidation at the purines through type I mechanism. The presence of a methoxy group at C(7) enhances the photosensitizing properties of **1** either by increasing its binding affinity with ctDNA and/or by increasing its oxidation potential. This agrees with the fact that **1** showed a selective damage profile where oxidised purines represent the main type of DNA photoproducts formed. In the case of **2**, single-strand breaks (SSBs) in addition to DNA oxidative damage are mostly induced. In this case, a concerted hydrolytic attack (due to a strong pH change in the surroundings of the DNA chain triggered by photoexcited **2**) is suggested as an additional mechanism accounting for the SSBs formation.

(ii) Both DHβCs as well as the full-aromatic derivatives **3** and **4** show quite a strong intracellular accumulation into different compartments of HeLa cells including lysosomes, endoplasmic reticulum and to a lower extent mitochondria. Interestingly, nuclear

accumulation of **1** – **4** was also observed being the later fact more evident for those βCs bearing a hydroxyl group (*i.e.*, **2** and **4**). Interestingly, the four βCs investigated herein showed a distinctive internalisation pattern with respect to the quaternary (cationic) *2*,*9*-dimethyl-βC reported by Denofrio *et al.* [16] that mainly accumulates into mitochondria. Targeting key cell's compartments (including the lysosomes) with photoactive molecules represent an emerging strategy for Photodynamic Therapy. For all the compounds, lifetime changes depending on the subcellular domain. This can have particular ramifications in the development of biotechnological tools based on small molecules derived from βC alkaloids. [52]

(iii) The non-negligible mitochondrial colocalization of **1** and **2** reported herein would support the hypothesis formulated by Lee *et al.* [14] suggesting that the neuroprotective role observed for these two alkaloids would occur at the submitochondrial domain. In addition, since monoamine oxidase enzymes (MAO) are located in the external membrane of mitochondria, DHβCs would still exert their enzyme inhibitory effect reported. [16]

(iv) Both DHβCs (**1** and **2**) showed lower cytotoxicity on eukaryotic cell culture than the corresponding full-aromatic derivatives **3** and **4**. However, among the two DHβCs, **2** was less cytotoxic than **1**.

(v) Upon photoexcitation, **1** showed a strong photodynamic effect, whereas **2** did not show any effect under the experimental conditions explored herein. This fact is interpreted herein as a manifestation of the distinctive photosensitized DNA-damage profiles and photooxidative extent shown by both DHβCs (*i. e.*, purine oxidation and AP-sites vs. single-strand breaks in the case of **1** and **2**, respectively). Thus, distinctive oxidative damage (either on genetic material or other biologically relevant targets) can be photoinduced, triggering distinct biochemical processes. [50] The slightly different internalisation pattern can also play a role.

(vi) The understanding of the photosensitizing properties of DHβCs in a biological environment lies not only on their biological relevance, but also in the fact that these alkaloids have been suggested as potential therapeutic drugs. In particular, the potential use of **1** and **2** in hypopigmentation skin disorders was suggested. [13] In this context, the rather low or null efficiency of reactive oxygen production (*i. e.*, singlet oxygen, $\Phi_{\Delta} \sim 0.02$) reported for compound **2**, [23] in addition to its very low cytotoxicity ($CC_{50} > 600$ μM) as well as the lack of intracellular photodynamic activity reported herein, indicate that **2** (harmalol) would be the best candidate for this particular pharmacological application.

ACKNOWLEDGEMENTS

The present work was partially supported by Grants PICT 2018-3193 (ANPCyT, Argentina), CTQ2017-85658-R and CTQ2014-55474-C2-2-R (Spanish Ministry of Economy and Competitiveness), A-CTS-186-UGR20 and A-FQM-230-UGR20 (Junta de Andalucía (I+D+I project within the FEDER Operational program). MPD and FMC are research members of CONICET. Authors want to thank Lic. Nadia Gomez-Olave for his assistance in the cytotoxicity experiments, as well as Dr. Ronald Vargas and Dr. Bernd Epe for their careful reading of the text and their valuable contributions in the discussions regarding the electrochemical and the DNA damage analysis, respectively.

CONFLICT OF INTEREST

On behalf of all authors, the corresponding authors state that there is no conflict of interest.

REFERENCES

[1] R. Zayed, M. Wink, Î²-Carboline and quinoline alkaloids in root cultures and intact plants of Peganum harmala, Zeitschrift fur Naturforschung - Section C Journal of Biosciences, 60 (2005) 451-458.
[2] Y.H. Wang, V. Samoylenko, B.L. Tekwani, I.A. Khan, L.S. Miller, N.D. Chaurasiya, M.M. Rahman, L.M. Tripathi, S.I. Khan, V.C. Joshi, F.T. Wigger, I. Muhammad, Composition, standardization and chemical profiling of Banisteriopsis caapi, a plant for the treatment of neurodegenerative disorders relevant to Parkinson's disease, Journal of Ethnopharmacology, 128 (2010) 662-671.
[3] S.J. Stachell, S.A. Stockwell, D.L. Van Vranken, The fluorescence of scorpions and cataractogenesis, Chem. Biol., 6 (1999) 531-539.
[4] C. Liu, M.N. Masuno, J.B. MacMillan, T.F. Molinski, Enantioselective Total Synthesis of (+)-Milnamide A and Evidence of Its Autoxidation to (+)-Milnamide D, Angew. Chem. Int. Ed., 43 (2004) 5951-5954.
[5] N. Cao, C.H. Wang, Strictosidine synthase, an indispensable enzyme involved in the biosynthesis of terpenoid indole and β-carboline alkaloids, Chin J Nat Med, 19 (2021) 591-607.
[6] F. Villarruel, M.P. Denofrio, F.A.O. Rasse-Suriani, F.S. García Einschlag, T. Schmidt De León, R. Erra-Balsells, F.M. Cabrerizo, Light-induced full aromatization and hydroxylation of 7-methoxy-1-methyl-3,4-dihydro-2H-pyrido[3,4-b]indole alkaloid: Oxygen partial pressure as a key modulator of the photoproducts distribution, J. Photochem. Photobiol. B., 199 (2019) 111600.
[7] R. Cao, W. Peng, Z. Wang, A. Xu, b-carboline alkaloids: Biochemical and pharmacological functions, Curr. Med. Chem., 14 (2007) 479-500.
[8] G.M. Olmedo, L. Cerioni, M.M. González, F.M. Cabrerizo, V.A. Rapisarda, S.I. Volentini, Antifungal activity of b-carbolines on Penicillium digitatum and Botrytis cinerea, Food Microbiology, 62 (2017) 9-14.
[9] G.M. Olmedo, L. Cerioni, M.M. González, F.M. Cabrerizo, S.I. Volentini, V.A. Rapisarda, UVA Photoactivation of Harmol Enhances Its Antifungal Activity against the Phytopathogens Penicillium digitatum and Botrytis cinerea, Frontiers in Microbiology, 8 (2017).
[10] M.M. Gonzalez, F.M. Cabrerizo, A. Baiker, R. Erra-Balsells, A. Osterman, H. Nitschko, M.G. Vizoso-Pinto, b-Carboline derivatives as novel antivirals for herpes simplex virus, Int. J. Antimicrob. Ag., 52 (2018) 459-468.
[11] F.A. Khan, A. Maalik, Z. Iqbal, I. Malik, Recent pharmacological developments in β-carboline alkaloid “harmaline”, European Journal of Pharmacology, 721 (2013) 391-394.
[12] M.A.M. El Gendy, A.A. Soshilov, M.S. Denison, A.O.S. El-Kadi, Harmaline and harmalol inhibit the carcinogen-activating enzyme CYP1A1 via transcriptional and posttranslational mechanisms, Food. Chem. Toxicol., 50 (2012) 353-362.
[13] S.Y. Park, Y.H. Kim, G. Park, S.J. Lee, Beta-carboline alkaloids harmaline and harmalol induce melanogenesis through p38 mitogen-activated protein kinase in B16F10 mouse melanoma cells, BMB Reports, 43 (2010) 824-829.
[14] C.S. Lee, E.S. Han, Y.Y. Jang, J.H. Han, H.W. Ha, D.E. Kim, Protective effect of harmalol and harmaline on MPTP neurotoxicity in the mouse and dopamine-induced damage of brain mitochondria and PC12 cells, Journal of neurochemistry, 75 (2000) 521-531.
[15] M.L. Alomar, J.G. Yañuk, S.O. Angel, M.M. Gonzalez, F.M. Cabrerizo, In vitro effect of harmine alkaloid and its N-methyl-derivatives against Toxoplasma gondii, Front. Microbiol., 12 (2021).
[16] M.P. Denofrio, F.A.O. Rasse-Suriani, J.M. Paredes, F. Fassetta, L. Crovetto, M.D. Giron, R. Salto, B. Epe, F.M. Cabrerizo, N-Methyl-β-carboline alkaloids: structure-dependent photosensitizing properties and localization in subcellular domains, Org. Biomol. Chem., 18 (2020) 6519-6530.
[17] M.M. Gonzalez, J. Arnbjerg, M. Paula Denofrio, R. Erra-Balsells, P.R. Ogilby, F.M. Cabrerizo, One- and two-photon excitation of b-carbolines in aqueous solution: pH-dependent spectroscopy, photochemistry, and photophysics, J. Phys. Chem. A, 113 (2009) 6648-6656.
[18] F.A.O. Rasse-Suriani, F.S. García-Einschlag, M. Rafti, T. Schmidt De León, P.M. David Gara, R. Erra-Balsells, F.M. Cabrerizo, Photophysical and Photochemical Properties of Naturally Occurring normelinonine F and Melinonine F Alkaloids and Structurally Related N(2)- and/or N(9)-methyl-β-carboline Derivatives, Photochem. Photobiol., 94 (2018) 36-51.
[19] M.M. Gonzalez, M. Vignoni, M. Pellon-Maison, M.A. Ales-Gandolfo, M.R. Gonzalez-Baro, R. Erra-Balsells, B. Epe, F.M. Cabrerizo, Photosensitization of DNA by b-carbolines: Kinetic analysis and photoproduct characterization, Org. Biomol. Chem., 10 (2012) 1807-1819.
[20] M. Vignoni, R. Erra-Balsells, B. Epe, F.M. Cabrerizo, Intra- and extra-cellular DNA damage by harmine and 9-methyl-harmine, J. Photochem. Photobiol. B., 132 (2014) 66-71.
[21] M. Vignoni, F.A.O. Rasse-Suriani, K. Butzbach, R. Erra-Balsells, B. Epe, F.M. Cabrerizo, Mechanisms of DNA damage by photoexcited 9-methyl-β-carbolines, Org. Biomol. Chem., 11 (2013) 5300-5309.

[22] J.G. Yañuk, M.P. Denofrio, F.A.O. Rasse-Suriani, F.D. Villarruel, F. Fassetta, F.S. García Einschlag, R. Erra-Balsells, B. Epe, F.M. Cabrerizo, DNA damage photo-induced by chloroharmine isomers: hydrolysis versus oxidation of nucleobases, Org. Biomol. Chem., 16 (2018) 2170-2184.
[23] F.D. Villarruel, M.P. Denofrio, R. Erra-Balsells, E. Wolcan, F.M. Cabrerizo, Photophysical and spectroscopic features of 3,4-dihydro-β-carbolines: a combined experimental and theoretical approach, Phys. Chem. Chem. Phys., 22 (2020) 20901-20913.
[24] J.G. Yañuk, F.D. Villarruel, M.L. Alomar, F.A.O. Rasse-Suriani, M.M. Gonzalez, E. Gonik, L. Madriz, R. Vargas, R. Erra-Balsells, M.P. Denofrio, F.M. Cabrerizo, Current landscape of the spectroscopic and photochemical properties of β-Carboline alkaloids in aqueous media towards understanding their biological role. REVIEW, An. Asoc. Quim. Argent., 107 (2021) 186-229.
[25] M. Salditt, S.N. Braunstein, R.D. Camerini-Otero, R.M. Franklin, Structure and synthesis of a lipid-containing bacteriophage: X. Improved techniques for the purification of bacteriophage PM2, Virology, 48 (1972) 259-262.
[26] S. Boiteux, T.R. O'Connor, F. Lederer, A. Gouyette, J. Laval, Homogeneous Escherichia coli FPG protein. A DNA glycosylase which excises imidazole ring-opened purines and nicks DNA at apurinic/apyrimidinic sites, Journal of Biological Chemistry, 265 (1990) 3916-3922.
[27] E. Müller, S. Boiteux, R.P. Cunningham, B. Epe, Enzymatic recognition of DNA modifications induced by singlet oxygen and photosensitizers, Nucleic Acids Research, 18 (1990) 5969-5973.
[28] M.M. Gonzalez, F.A.O. Rasse-Suriani, C.A. Franca, R. Pis Diez, Y. Gholipour, H. Nonami, R. Erra-Balsells, F.M. Cabrerizo, Photosensitized electron transfer within a self-assembled norharmane–2′-deoxyadenosine 5′-monophosphate (dAMP) complex, Org. Biomol. Chem., 10 (2012) 9359-9372.
[29] B. Epe, DNA damage spectra induced by photosensitization, Photochem. Photobiol. Sci., 11 (2012) 98-106.
[30] J. Schindelin, I. Arganda-Carreras, E. Frise, V. Kaynig, M. Longair, T. Pietzsch, S. Preibisch, C. Rueden, S. Saalfeld, B. Schmid, J.-Y. Tinevez, D.J. White, V. Hartenstein, K. Eliceiri, P. Tomancak, A. Cardona, Fiji: an open-source platform for biological-image analysis, Nature Methods, 9 (2012) 676-682.
[31] M.M. Gonzalez, M. Pellon-Maison, M.A. Ales-Gandolfo, M.R. Gonzalez-Baró, R. Erra-Balsells, F.M. Cabrerizo, Photosensitized cleavage of plasmidic DNA by norharmane, a naturally occurring b-carboline, Org. Biomol. Chem., 8 (2010) 2543-2552.
[32] M.M. Gonzalez, M.P. Denofrio, F.S. Garcia Einschlag, C.A. Franca, R. Pis Diez, R. Erra-Balsells, F.M. Cabrerizo, Determining the molecular basis for the pH-dependent interaction between 2'-deoxynucleotides and 9H-pyrido[3,4-b]indole in its ground and electronic excited states, Phys. Chem. Chem. Phys., 16 (2014) 16547-16562.
[33] K. Butzbach, F.A.O. Rasse-Suriani, M.M. Gonzalez, F.M. Cabrerizo, B. Epe, Albumin–Folate Conjugates for Drug-targeting in Photodynamic Therapy, Photochem. Photobiol., 92 (2016) 611-619.
[34] J.G. Yañuk, M.L. Alomar, M.M. Gonzalez, F. Simon, R. Erra-Balsells, M. Rafti, F.M. Cabrerizo, DNA damage induced by bare and loaded microporous coordination polymers from their ground and electronic excited states, Phys. Chem. Chem. Phys., 17 (2015) 12462-12465.
[35] I. Maisuls, F.M. Cabrerizo, P.M. David-Gara, B. Epe, G.T. Ruiz, DNA Oxidation Photoinduced by Norharmane Rhenium(I) Polypyridyl Complexes: Effect of the Bidentate N,N′-Ligands on the Damage Profile, Chemistry – A European Journal, 0 (2018).
[36] S. Sarkar, P. Pandya, K. Bhadra, Sequence Specific Binding of Beta Carboline Alkaloid Harmalol with Deoxyribonucleotides: Binding Heterogeneity, Conformational, Thermodynamic and Cytotoxic Aspects, PLOS ONE, 9 (2014) e108022.
[37] Z. Taira, S. Kanzawa, C. Dohara, S. Ishida, M. Matsumoto, Y. Sakiya, Intercalation of Six β-Carboline Derivatives into DNA Jap. J. Toxicol. Environ. Health, 43 (1997) 83-91.
[38] V. Lhiaubet-Vallet, M.C. Cuquerella, J.V. Castell, F. Bosca, M.A. Miranda, Triplet Excited Fluoroquinolones as Mediators for Thymine Cyclobutane Dimer Formation in DNA, The Journal of Physical Chemistry B, 111 (2007) 7409-7414.
[39] G. Duportail, H. Lami, Studies of the interaction of the fluorophores harmine and harmaline with calf thymus DNA, Biochimica et Biophysica Acta (BBA) - Nucleic Acids and Protein Synthesis, 402 (1975) 20-30.
[40] G. Duportail, Linear and circular dichroism of harmine and harmaline interacting with DNA, Int. J. Biol. Macromol., 3 (1981) 188-192.
[41] M. Caprasse, C. Houssier, Do planar alkaloids from Strychnos usambarensis intercalate into the DNA helix?, Biochimie, 65 (1983) 157-167.
[42] S. Nafisi, M. Bonsaii, P. Maali, M.A. Khalilzadeh, F. Manouchehri, b-Carboline alkaloids bind DNA, J. Photochem. Photobiol. B., 100 (2010) 84-91.
[43] S. Sarkar, K. Bhadra, Binding of alkaloid harmalol to DNA: Photophysical and calorimetric approach, J. Photochem. Photobiol. B., 130 (2014) 272-280.
[44] R. Sahoo, R. Jana, D. Seth, Photophysics of harmaline in solvent mixtures, Journal of Molecular Liquids, 275 (2019) 84-90.
[45] I. Ayoob, Y.M. Hazari, S.H. Lone, Shakeel-u-Rehman, M.A. Khuroo, K.M. Fazili, K.A. Bhat, Phytochemical and Cytotoxic Evaluation of Peganum Harmala: Structure Activity Relationship Studies of Harmine, ChemistrySelect, 2 (2017) 2965-2968.
[46] S. Roy, T. Mohammad, P. Gupta, R. Dahiya, S. Parveen, S. Luqman, G.M. Hasan, M.I. Hassan, Discovery of Harmaline as a Potent Inhibitor of Sphingosine Kinase-1: A Chemopreventive Role in Lung Cancer, ACS Omega, 5 (2020) 21550-21560.
[47] A. Abe, H. Yamada, Harmol induces apoptosis by caspase-8 activation independently of Fas/Fas ligand interaction in human lung carcinoma H596 cells, Anticancer Drugs, 20 (2009) 373-381.
[48] R. Cao, Q. Chen, X. Hou, H. Chen, H. Guan, Y. Ma, W. Peng, A. Xu, Synthesis, acute toxicities, and antitumor effects of novel 9-substituted b-carboline derivatives, Bioorganic and Medicinal Chemistry, 12 (2004) 4613-4623.
[49] T. Ghosh, S. Sarkar, P. Bhattacharjee, G.C. Jana, M. Hossain, P. Pandya, In vitro relationship between serum protein binding to beta-carboline alkaloids: a comparative cytotoxic, spectroscopic and calorimetric assays, 38 (2020) 1103-1118.
[50] T.M. Tsubone, W.K. Martins, M.S.F. Franco, M.N. Silva, R. Itri, M.S. Baptista, Cellular compartments challenged by membrane photo-oxidation, Archives of Biochemistry and Biophysics, 697 (2021) 108665.
[51] D. Kessel, Apoptosis, Paraptosis and Autophagy: Death and Survival Pathways Associated with Photodynamic Therapy, Photochem. Photobiol., 95 (2019) 119-125.
[52] S. Hotha, J.C. Yarrow, J.G. Yang, S. Garrett, K.V. Renduchintala, T.U. Mayer, T.M. Kapoor, HR22C16: A Potent Small-Molecule Probe for the Dynamics of Cell Division, Angew. Chem. Int. Ed., 42 (2003) 2379-2382.

GRAPHICAL ABSTRACT

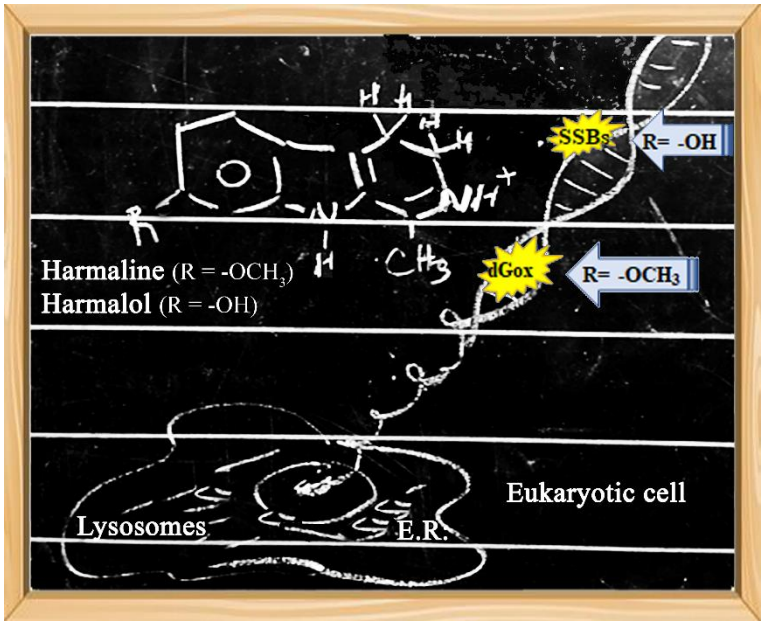

The subtle structural difference (*i. e.*, the exchange of a methoxy group for a hydroxyl substituent at C(7)) between harmaline and harmalol, gives rise to distinctive photosensitizing and subcellular localization pattern.